# Control Co-Design of Mechanical Power Takeoff for a Dual-flap Surge Wave Energy Converter

Lisheng Yang\*, Jia Mi\*, Jianuo Huang\*, Giorgio Bacelli<sup>†</sup>, Muhammad Hajj<sup>‡</sup> and Lei Zuo\*

\*Department of Naval Architecture and Marine Engineering,

University of Michigan, Ann Arbor, Michigan 48109, USA Email: leizuo@umich.edu

†Sandia National Laboratories, Albuquerque, 87185, USA Email: gbacell@sandia.gov

‡Department of Civil, Environmental and Ocean Engineering

Stevens Institute of Technology, Hoboken, NJ 07030, USA Email: mhajj@stevens.edu

Abstract—This paper presents a control co-design method for designing mechanical power takeoff (PTO) systems of wave energy converters. A dual-flap oscillating surge wave energy converter is selected to carry out the two degrees of freedom co-design investigation. Unlike most existing work's simplified representation of harvested power, this paper derives a more realistic electrical power representation based on a concise PTO modelling. This electrical power is used as the objective for PTO design optimization with energy maximization control also taken into consideration to enable a more comprehensive design evaluation. A simple PI control structure speeds up the simultaneous co-optimization of control and PTO parameters, and an equivalent circuit model of the WEC not only streamlines power representation but also facilitates more insightful evaluation of the optimization results. The optimized PTO shows a large improvement in terms of power potential and actual power performance. It's found the generator's parameters have the most influences on the power increase.

# I. INTRODUCTION

Oscillating surge wave energy converters (OSWEC), often designed in a flap-akin shape, have seen several successful deployments in the past two decades [1], [2]. However, most of those projects are designed for deployment in nearshore waters, which have less wave power potential than offshore waters. One of the biggest challenges for OSWEC in offshore waters is the mooring cost, which is estimated to take up more than 50 of the total installation cost in one study [3]. Recently, a dual-flap OSWEC with a floating platform is proposed to reduce the needed mooring loads [4]. Two wave capture flaps are placed on a floating platform at a distance of roughly half wavelength away from each other. They are designed to move largely out of phase so that the horizontal surge forces on the platform are largely cancelled. This paper discusses the mechanical power takeoff (PTO) control codesign for such a dual-flap OSWEC. Specifically, the mechanical transmission coefficients and generator coefficients are designed along with a PI feedback controller to maximize electrical energy generation for a particular wave spectrum. Conventionally, control design is the last step in the WEC development process and is conducted after the power takeoff parameters have been fixed. However, recent studies [5] show such an approach limits the real power performance of the WEC. The reason is that most previous studies neglect detailed PTO dynamics and use an oversimplified representation for

power. This oversimplification is observed both in the WEC hydrodynamics community (such as [6]) and WEC control community (such as [7]). Due to the complexities of their respective research objects, the mechanical power conveniently represented by force times velocity is taken as an indicator of harvested power. But the ultimate usable power is the electrical power output of the generator, not the input mechanical power to the PTO system. When considering the electrical power, the reactive control commonly used in WEC control [8] is no longer loss free. Resistive dissipation is always incurred anytime currents are applied to the generator to produce force. Therefore, it's no longer the best option to directly draw generator currents (which is how control is applied) whenever reactive power is needed. Instead, the mechanical transmission can serve as physical reactive components without suffering from the dissipation losses incurred by applying control. The conceptual design of those reactive components, including transmission inertia and stiffness, is crucial to achieving the maximal useful electrical energy generation.

In this paper, the design of mechanical transmission and generator coefficients is considered simultaneously with the design of control gains of a feedback controller. The hydrodynamic model of the dual-flap, the mechanical transmission model and the electrical generator model of the PTO are integrated into an equivalent circuit representation using the framework developed in [9]. Then the electrical power formulation is derived based on the equivalent circuit. Numerical optimization is used to optimize the electrical power over the design and control coefficients under constraints. Critical comparisons are drawn between cases with optimal and suboptimal design coefficients to illustrate the importance of proper mechanical components design. In addition, the corresponding equivalent circuit values are evaluated to find out individual parameters that have the most influences on power potential enhancement, providing a guidance to components selection.

The paper is organized as follows. Section 2 describes the design and modelling of the dual-flap OSWEC's wave capture structure. Section 3 first presents the detailed modelling of the PTO system, then derives the equivalent circuit representation of the overall WEC and next the control co-design problem is formulated. Section 4 shows and discusses the optimization results while section 5 concludes the paper.

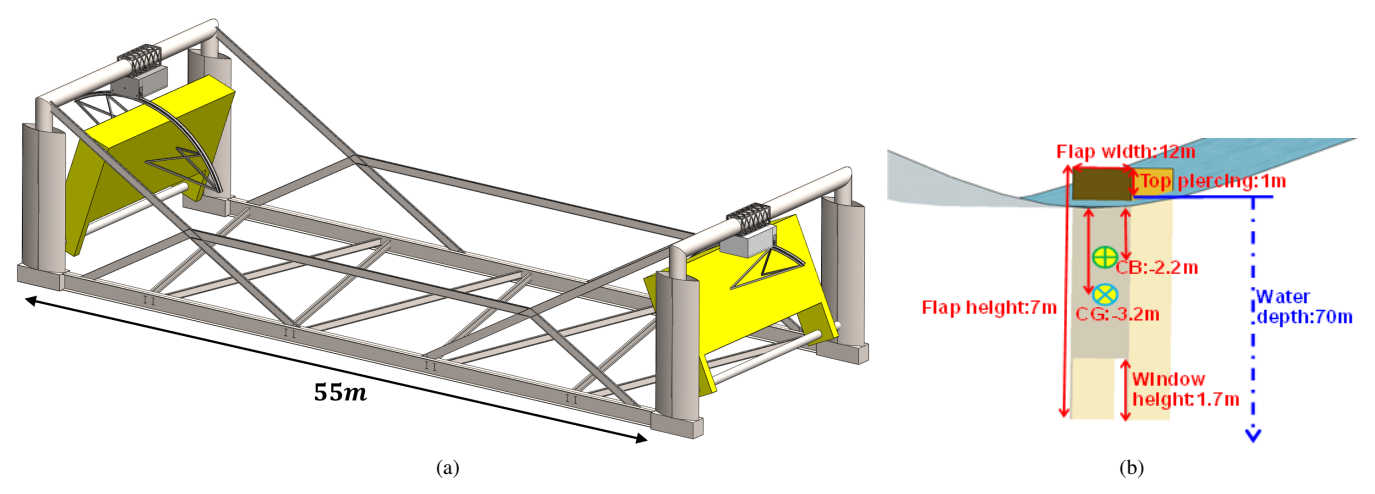


Fig. 1. (a) Overall self-balancing OSWEC structure; (b) The dimension and property of the flap

### II. OVERVIEW OF SELF-BALANCING DUAL-FLAP OSWEC

The overall structure of the designed dual-flap oscillating surge wave energy converter is shown in Fig. 1a. The key design parameter here is the length between the forward and aft flaps which determines the phase difference between their wave excitation forces. Here a 55m length is chosen as roughly half the wavelength of the dominant wave frequency so that the two flaps have a 180 degree phase difference in their wave excitation. The wave capture flaps are tuned in shape to have an in-phase motion with the wave excitation force around the dominant frequency. The dimensions of the flaps are the same and shown in Fig. 1b, thus around the dominant wave frequency the two flaps will largely move out of phase. In this way, the horizontal forces the flaps place on the floating support trusses can be largely cancelled and the mooring requirement for the device decreases accordingly.

The designed power takeoff for this WEC is based on mechanical transmission and the flaps' pitch motion is primarily used to take out power while other degrees of freedom are constrained by the support structures and the mooring. A novel belt transmission system in the PTO is used to directly transmit the flaps' pitch rotation to the high speed rotation of a generator. In this sense, both the wave surge force and the generator torque act on the flap as an equivalent torque pivoting around its bottom hinge, and from now on we will call any force in terms of its equivalent torque. Then, the dual-flaps' motion equation can be written out in the frequency domain as:

$$\begin{bmatrix} T_{ex}^{1}(\omega) + T_{pto}^{1}(\omega) \\ T_{ex}^{2}(\omega) + T_{pto}^{2}(\omega) \end{bmatrix} = \begin{bmatrix} Z_{i}^{11} & Z_{i}^{12} \\ Z_{i}^{21} & Z_{i}^{22} \end{bmatrix} \begin{bmatrix} V^{1}(\omega) \\ V^{2}(\omega) \end{bmatrix}$$
(1)

Here  $Z_i$  is the intrinsic impedance matrix of the dual-flaps, which dictates how the two flaps will move subject to external torques. This intrinsic impedance depends on both the flap shape's hydrodynamics properties and the flaps' mechanical properties. Specifically, in the frequency domain, radiation

torque induced by one flap's motion can be expressed as:

$$T_{Rad}^{ji} = -(B_{ji} + j\omega A_{ji})V_i \tag{2}$$

If j=i,  $B_{ji}$  and  $A_{ji}$  are equal to a damping and an inertia term, thus the so-called radiation damping and added inertia. They need to be combined with the flap's mechanical damping and moment of inertia for writing out the impedance expression. In addition, the hydro-static torque which comes from buoyancy and gravity is usually simply modelled as a spring torque in proportion to the flap's displacement from the equilibrium. In the proposed dual-flap configuration, the two flaps' hydro-static torques are independent, with the same hydro-stiffness:

$$T_{static}^{i} = -K \frac{V_{i}}{j\omega} \tag{3}$$

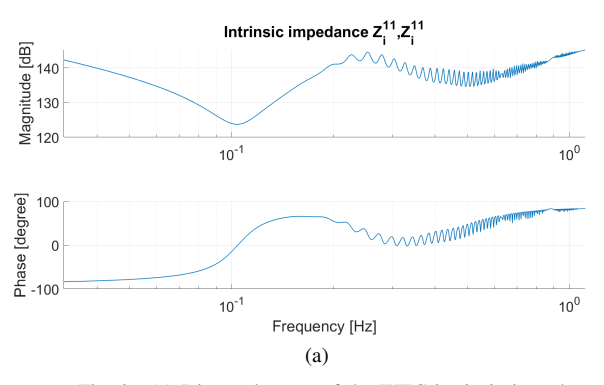
Then it can be easily shown that for diagonal terms of the impedance matrix:

$$Z_i^{ii} = B_{ii} + B_f + j\omega(I_f + A_{ii} - \frac{K}{\omega^2})$$
 (4)

Where  $B_f$  and  $I_f$  are the flap's own mechanical damping and inertia, which are identical for the two flaps. The off-diagonal terms describe the coupling effects between the two flaps and only depend on the radiation effects in this case:

$$Z_i^{ji} = B_{ji} + j\omega A_{ji} \tag{5}$$

For the proposed design discussed in this paper, the WEC's intrinsic impedance is taken as given and fixed. It is calculated from boundary element method (BEM) software Nemoh and estimation of the flaps' mechanical properties. Due to the duplicate shape and symmetric layout,  $Z_i^{11} = Z_i^{22}$  and  $Z_i^{12} = Z_i^{21}$ . The bode diagrams of the self and cross impedance are shown in Fig. 2. The noisier results at higher frequency ranges are caused by the numerical computation of the BEM solver. Since the sea condition the WEC is designed for has most energy concentrated around 5 to 15 seconds (0.2 to 0.06 Hz), the noisy effects at higher frequency are deemed not important.



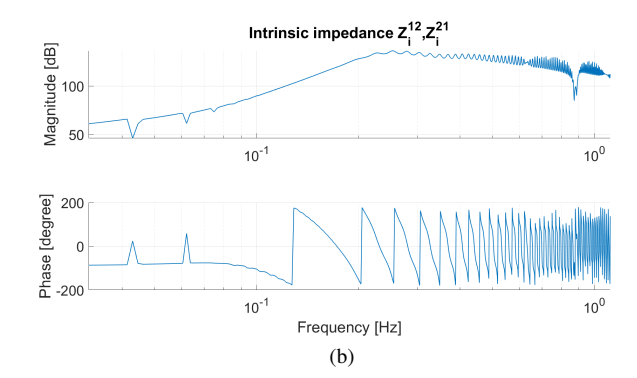


Fig. 2. (a) Diagonal terms of the WEC intrinsic impedance matrix; (b) Off-diagnonal terms of the WEC intrinsic impedance matrix

#### III. MECHANICAL PTO CONTROL CO-DESIGN

Most WEC control literature so far directly takes  $T_{pto}$  in Equation 1 as the control variable, and takes  $-T_{pto} * V$  as the control objective, which is the mechanical energy transmitted to the PTO system. In practice, however,  $T_{pto}$  has to be applied through some actuators and transmission components, and the mechanical energy absorbed into the PTO is not equal to the energy delivered to the generator. Moreover, the generator itself incur different losses depending on its operation conditions, and the ultimate usable power is thus different from the mechanical power at the generator shaft. Therefore, the mechanical energy absorbed by PTO system  $-T_{pto} * V$  is a poor indicator of the device's actual performance. Instead, the control objective should be the output electrical energy from the generator to its load. To maximize this electrical power, the dynamics of the PTO transmission and generator is no longer negligible. Furthermore, it will be shown the design and selection of these PTO components could have significant impacts on the control performance. And a control co-design method is needed to choose the optimal PTO parameters for a given wave capture structure.

# A. PTO Mechanical Transmission Modelling

In the proposed design PTO transmission is purely composed of mechanical components for ease of maintenance and operation. That means the generator is directly connected to the flap except for some gear stages N as shown in Fig. 3. In our design, most of the gear ratio is achieved by the diameter ratio between the arch on top of the flap and the small pulley connected to the generator driveshaft. The manufacturing cost and reliability of the transmission system largely depend on the selection of this gear ratio. Moreover, since the flap's rotational velocity range is determined by the wave frequency, the transmission gear ratio directly affects the velocity range of the generator. Hence, at an early conceptual design stage, we only model the essential parts of the transmission as a lumped inertia  $I_g$ , a lumped damping  $B_g$  and a lumped gear ratio N to evaluate the influences of these fundamental parameters.

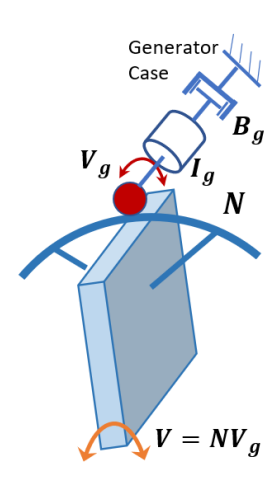


Fig. 3. Mechanical transmission modelling

# B. PTO Generator Modelling

The generator chosen for the PTO is a permanent magnet synchronous machine (PMSM). While the exact dynamics modelling of a PMSM can get as complicated as needed, here only the most essential parts are considered for simplicity. As shown in Fig. 4, the generator is modelled as an equivalent RL circuit. For PMSM, this is made possible by transforming phase voltages and currents to the rotor reference frame of direct and quadrature (dq) axes. As flux weakening wouldn't be needed for most operation conditions, the direct axis current is assumed to always be controlled to 0. Then all the electrical energy is delivered to the load from the quadrature axis current

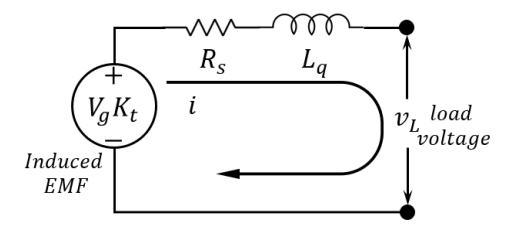


Fig. 4. Generator equivalent circuit

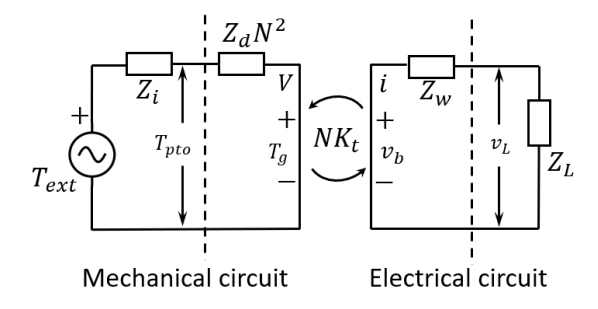


Fig. 5. Circuit modelling of the entire WEC system

 $i_q$ . The q axis circuit has two voltage sources: the induced electromagnetic force (EMF) and an external load voltage. To equalize mechanical and electrical energy, the voltage and current of the q axis circuit need to be scaled for the sake of energy conservation. Thus the resulting circuit cannot be viewed as only the q axis circuit but more of a DC motor equivalent of the PMSM. Still, as current and voltage can be scaled by the same factor, the passive components including the stator resistance  $R_s$  and q axis inductance  $L_q$  remain the same. Note that this model only considers the copper losses since core losses are typically much less in below rated speed operations.

# C. Dual-flap WEC Circuit Modelling

Based on the modelling assumptions introduced in the above sections, an overall model of the dual-flap WEC can be conveniently represented as a hybrid circuit. As shown in Fig. 5, the mechanical circuit has the wave excitation torque as a voltage source, and the flaps' rotational velocity V is the resulting current. When the generator draws a current, a generator torque  $T_q$  is applied acting as another voltage source to the mechanical circuit. Note that  $T_q$  is amplified by N so that the mechanical circuit's current — the velocity of the flaps, remains consistent. Similar amplification is applied to the mechanical transmission impedance  $Z_d = B_q + j\omega I_q$ . On the electrical circuit side, generator winding impedance  $Z_w$  is defined as  $R_s + j\omega L_q$ . The load impedance determines the actual electrical energy output  $v_L i = Z_L i^2$ . The control algorithm, which seeks to maximize this electrical output, determines  $Z_L$ . The implementation of  $Z_L$  is left to power electronics and assumed to be accurately implementable for this study. The coupling between the mechanical and electrical circuits is through the the generator's torque constant  $K_t$  and the gear ratio N. The fundamental equation relating the two side of the PTO can be written as a linear transform:

$$\begin{bmatrix} \mathbf{T_{pto}} \\ \mathbf{v_L} \end{bmatrix} = \begin{bmatrix} -\mathbf{Z_{11}} & \mathbf{Z_{12}} \\ \mathbf{Z_{21}} & -\mathbf{Z_{22}} \end{bmatrix} \begin{bmatrix} \mathbf{V} \\ \mathbf{i} \end{bmatrix} \tag{6}$$

Here all variables are duple involving two degrees of freedom of the dual-flaps. Specifically,  $\mathbf{T_{pto}} = [T^1_{pto}(\omega), T^2_{pto}(\omega)]^T$ ,  $\mathbf{V} = [V^1(\omega), V^2(\omega)]^T$ ,  $\mathbf{v_L} = [v^1_L(\omega), v^2_L(\omega)]^T$  and  $\mathbf{i} = [i^1(\omega), i^2(\omega)]^T$ . The submatrices of the PTO impedance are

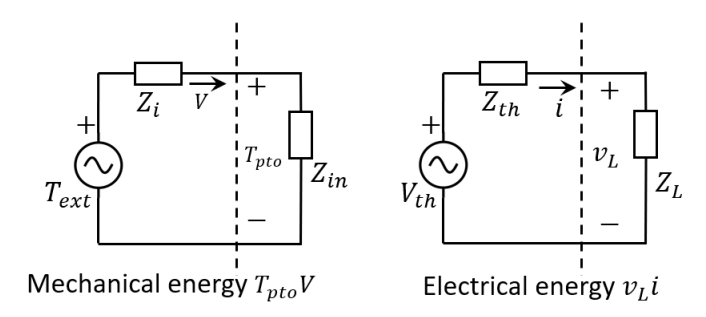


Fig. 6. Thévenin equivalent circuits for the WEC

all diagonal matrices due to the independent nature of the two sets of PTO. Their values are:

$$\mathbf{Z_{11}} = \begin{bmatrix} Z_d^1 N_1^2 & 0\\ 0 & Z_d^2 N_2^2 \end{bmatrix}$$
 (7a)

$$\mathbf{Z_{12}} = \begin{bmatrix} -K_t^1 N_1 & 0\\ 0 & -K_t^2 N_2 \end{bmatrix}$$
 (7b)

$$\mathbf{Z_{21}} = \begin{bmatrix} K_t^1 N_1 & 0\\ 0 & K_t^2 N_2 \end{bmatrix}$$
 (7c)

$$\mathbf{Z_{22}} = \begin{bmatrix} Z_w^1 & 0\\ 0 & Z_w^2 \end{bmatrix} \tag{7d}$$

## D. Thévenin Equivalent Circuits and Control Co-optimization

The hybrid circuit shown in Fig. 5 can be further condensed using the Thévenin's theorem. The resulting Thévenin Equivalent Circuit condensed at the terminals of the load is shown on the right side of Fig. 6. In this way the electrical power output can be easily derived as the active power delivered to the load. In contrast, the circuit on the left side of Fig. 6 is condensed at the terminals of the PTO. The input impedance of the PTO  $Z_{in}$  seen at this terminal port is determined by the PTO impedance and the load impedance. The active power delivered to this port is the mechanical power considered by many existing works. To derive expressions for  $Z_{in}$  and  $V_{th}$ ,  $Z_{th}$ , start with the governing equation of the WEC:

$$\mathbf{T_{ext}} + \mathbf{Z_{12}i} = (\mathbf{Z_i} + \mathbf{Z_{11}})\mathbf{V} \tag{8}$$

Note that generator current can be expressed as:

$$i = (Z_{22} + Z_L)^{-1}Z_{21}V$$
 (9)

Plug Equation 9 into 8, observe:

$$T_{\text{ext}} = (Z_i + Z_{11} - Z_{12}(Z_{22} + Z_L)^{-1}Z_{21})V$$
 (10)

It follows that:

$$Z_{in} = Z_{11} - Z_{12}(Z_{22} + Z_{L})^{-1}Z_{21}$$
 (11)

Alternatively, note the flaps' velocity can be expressed as:

$$V = Z_{21}^{-1}(Z_L + Z_{22})i$$
 (12)

Plug Equation 12 into 8, observe that:

$$\mathbf{Z_{21}}(\mathbf{Z_i} + \mathbf{Z_{11}})^{-1}\mathbf{T_{ext}} + \mathbf{Z_{21}}(\mathbf{Z_i} + \mathbf{Z_{11}})^{-1}\mathbf{Z_{12}}\mathbf{i}$$
  
=  $(\mathbf{Z_{22}} + \mathbf{Z_L})\mathbf{i}$  (13)

Then it's easy to see that:

$$V_{th} = Z_{21}(Z_i + Z_{11})^{-1}T_{ext}$$
 (14)

$$Z_{th} = Z_{22} - Z_{21}(Z_i + Z_{11})^{-1}Z_{12}$$
 (15)

For regular waves, the average electrical power for each frequency is then given as:

$$\overline{P_e} = \frac{1}{2} \Re \epsilon (\mathbf{i}^{\dagger} \mathbf{Z_L} \mathbf{i}) 
= \frac{1}{2} \Re \epsilon \left[ (\mathbf{V_{th}^{\dagger}} (\mathbf{Z_{th}} + \mathbf{Z_L})^{-\dagger} \mathbf{Z_L} (\mathbf{Z_{th}} + \mathbf{Z_L})^{-1} \mathbf{V_{th}} \right]$$
(16)

$$\overline{P_m} = \frac{1}{2} \mathfrak{Re}(\mathbf{\Omega}^{\dagger} \mathbf{Z_{in}} \mathbf{\Omega})$$

$$= \frac{1}{2} \mathfrak{Re} \left[ (\mathbf{T_{ext}^{\dagger}} (\mathbf{Z_i} + \mathbf{Z_{in}})^{-\dagger} \mathbf{Z_{in}} (\mathbf{Z_i} + \mathbf{Z_{in}})^{-1} \mathbf{T_{ext}} \right] (17)$$

As mentioned before,  $Z_L$  depends on the controller used for energy maximization. For this study, a simple PI controller is used to facilitate fast co-optimization. The controller is assumed to directly regulate PTO torque  $T_{pto}$  based on the flaps' velocity. Although in reality implementing this controller is challenging, it provides necessary control degree of freedom for the PTO co-design purpose. It's further assumed the control of the two flaps is independent, leading to a diagonal control impedance matrix:

$$\mathbf{T_{ext}} = \mathbf{Z_cV} = \begin{bmatrix} K_{P1} + \frac{K_{I1}}{j\omega} & 0\\ 0 & K_{P2} + \frac{K_{I2}}{j\omega} \end{bmatrix} \begin{bmatrix} V^1\\ V^2 \end{bmatrix} \quad (18)$$

As this controller is collocated at the terminals of the input impedance  $Z_{in}$  in Fig. 6, its relationship with  $Z_L$  can be found by the equation  $Z_c = -Z_{in}$ , which leads to the expression of  $Z_L$  as:

$$Z_{L} = Z_{21}(Z_{c} + Z_{11})^{-1}Z_{12} - Z_{22}$$
 (19)

Then the co-optimization problem is to maximize the average electrical power in Equation 17 over transmission parameters  $\{N_1,N_2,I_{g1},I_{g2}\}$ , generator parameters  $\{K_t^1,K_t^2,R_s^1,R_s^2,L_q^1,L_q^2\}$  and control parameters  $\{K_{P1},K_{P2},K_{I1},K_{I2}\}$ .

# IV. RESULTS

The proposed floating dual-flap OSWEC is designed specifically for the PacWave South test site. The wave spectrum used for this study is thus chosen as the most frequently occurring sea conditions for that test site. It's a JONSWAP spectrum with a 9 s dominant wave period and a 1.5m significant wave height. The wave energy spectrum is shown in Fig. 7 as the orange curve. The corresponding wave excitation torque spectrum is shown as the blue curves for both the forward and aft flaps. It can be seen the flaps show a rather broadband excitation profile with high excitation region extended from the peak frequency

TABLE I PTO PARAMETERS FOR OPTIMIZATION

	Nominal	Lower Bound	Upper Bound	Unit
Gear Ratio N	350	250	500	
Transmission Inertia $I_g$	10	5	20	${\rm Kgm^2}$
Torque constant $K_t$	6	3	9	Nm/A
Stator Resistance $R_s$	0.5	0.1	1	Ohm
Synchronous Inductance $L_q$	10	1	100	mH

TABLE II PTO OPTIMIZATION RESULTS

	Case 1	Case 2	Case 3	Case 4
Gear Ratio $N$	350	500	350	<u>290</u>
Transmission Inertia $I_g$	$10~{\rm Kgm^2}$	<b>5 Kgm</b> <sup>2</sup>	$10~{ m Kgm}^2$	$5~{ m Kgm}^2$
Torque constant $K_t$	6 Nm/A	6 Nm/A	9 Nm/A	9 Nm/A
Stator Resistance $R_s$	0.5 Ohm	0.5 Ohm	0.1 Ohm	0.1 Ohm
Synchronous Inductance $L_q$	10 mH	10 mH	<u>11.7 mH</u>	99.9 mH
Electrical Power $P_e$	18.6 kW	21.3 kW	26.2 kW	27 kW
Electrical Power Upper Bound $P_e^u$	20.1 kW	23.6 kW	36.3 kW	36.7 kW
Mechanical Power Upper Bound $P_m^u$	45.2 kW			

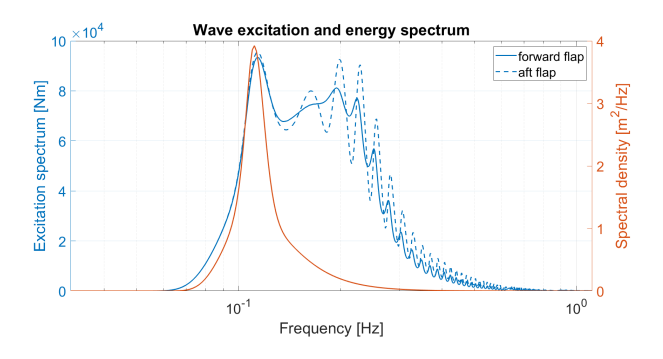


Fig. 7. Wave energy and excitation spectrum

well into higher frequency ranges despite of much less wave energy. And it shows the two flaps have similar excitation spectrum. Therefore, the same set of PTO parameters are adopted for the flaps, leading to 5 PTO parameters to be optimized as shown in Table I.

A total of four optimization cases are run to see the effects of co-design that take different PTO components into consideration. The optimization results are listed in Table II, where in case 1 only control parameters are optimized serving as the baseline, in case 2 both control and transmission parameters are optimized, in case 3 both control and generator

parameters are optimized, and in case 4 all parameters are cooptimized together.

The theoretical upper bounds of both electrical and mechanical energy can be conveniently obtained through the classic impedance matching condition. With the equivalent circuits shown in Fig. 6, the optimal electrical power is  $\frac{1}{8}V_{th}^{\dagger}\Re(Z_{th})^{-1}V_{th}$ , and the optimal mechanical power is  $\frac{1}{8}T_{ext}^{\dagger}\Re(Z_i)^{-1}T_{ext}$ . The optimization results show a 50% increase in actual electrical power and an 80% increase in electrical power potential when co-optimizing all five PTO parameters with control parameters together. This indicates the importance of applying co-design routine when selecting PTO components, because the main wave capture structure of the WEC only determines the theoretical maximum recoverable power. It requires a proper design of the PTO to fulfill as much of that theoretical potential as possible. By examining the optimal design parameters, it can be seen except for the gear ratio, other parameters are saturated to their limits. This indicates the possibility of further pushing the electrical power upper bound towards the mechanical power upper bound. However, expanding the limits may lead to physically hard to realize or uneconomic solutions. Therefore a balance needs to be stricken in choosing the parameter limits.

By examining the partial optimization cases 2 and 3, it can be seen optimizing generator parameters has more decisive effects than optimizing the transmission, with electrical power only increased marginally from case 3 to case 4. This may be due to the large added inertia typically associated with flap-like structures, leaving small room for the mechanical inertia to have an effect. Still, a co-optimization leads to much smaller gear ratio for similar power levels, which is important to reduce the cost.

The power and efficiency spectrums for case 1 and case 4 are shown in Fig. 8. The efficiencies are calculated against the mechanical power upper bounds. It is clearly seen the optimal PTO significantly increases the efficiency upper bound. With a low upper bound in case 1, even if the controller is optimized well and closely approaches the upper bound around the peak frequency region, the actual power is still much lower than case 4. Nevertheless, notice that in Fig. 8b there is still quite a margin to gain towards the PTO's electrical power limit. This indicates improvement margin for the controller. It's likely a more sophisticated controller may get even closer to the efficiency upper bound.

Lastly, to gain more insights into how the PTO optimization increases electrical power potential, it's helpful to plot out the Thévenin equivalent voltage and impedance to see how different PTOs shape these values. Fig. 9 shows the Thévenin impedance of case 1 and case 4. It can be seen that the optimal PTO slightly increases the impedance around the peak frequency but overall speaking the difference is very small across the entire spectrum. Also it's worth pointing out that the off-diagonal terms of the Thévenin impedance matrix is small enough to be neglected. This means that although the coupling effect between the two flaps through radiation is non-

negligible (as shown in Fig. 2b), this effect wouldn't have much influence on the actual power. In other words, the two flaps can be viewed as independent from the perspective of power generation. This property can be leveraged by later control design. Fig. 10 shows the Thévenin voltage magnitude for both cases. It turns out the optimized PTO design boosts power upper bound mainly through increasing the Thévenin voltage. Refer back to  $V_{th}$ 's expression in Equation 14, it can be seen that increasing  $K_t$  and decreasing  $I_g$  and N are means of increasing  $V_{th}$ . Also, from Fig. 10 we can see the equivalent voltages on both flaps' PTO are the same. This implies we can design controller for a single flap and use it for both.

#### V. CONCLUSION

In this paper, a fast control co-design method based on equivalent circuit representation of a wave energy converter is explained and used to optimize the mechanical PTO parameters of a dual-flap OSWEC. By considering key components including transmission and generator in the PTO, the proposed method directly targets the electrical energy output and thus is more practical in real world design problems. Meanwhile, a feedback PI controller is used to add control's degree of freedom in the early stage design problem, which provides more comprehensive evaluations of design choices. The simplicity of PI controller allows a fast co-optimization of both control and PTO parameters together, showing promise as an efficient way to evaluate more PTO parameters. The preliminary results show the optimized PTO significantly increases electrical energy upper bound, with the generator parameter optimization contributing the most to the increase for the considered OSWEC. Further analysis shows the optimized PTO increases energy by increasing the equivalent voltage on the load, highlighting the importance of generator torque constant and the transmission gear ratio.

### ACKNOWLEDGMENT

The authors would like to thank the financial support from US Department of Energy award No. DE-EE0008953 and US National Science Foundation award No. 2152694. In addition, we would also like to acknowledge the partial support from Sandia National Laboratories.

#### REFERENCES

- T. T. Loh, D. Greaves, T. Maeki, M. Vuorinen, D. Simmonds, and A. Kyte, "Numerical modelling of the waveroller device using openfoam," in *Proceedings of the 3rd Asian Wave & Tidal Energy Conference*, 2016.
- [2] T. Whittaker and M. Folley, "Nearshore oscillating wave surge converters and the development of oyster," *Philosophical Transactions of the Royal Society A: Mathematical, Physical and Engineering Sciences*, vol. 370, no. 1959, pp. 345–364, 2012.
- [3] Y.-H. Yu, D. Jenne, R. Thresher, A. Copping, S. Geerlofs, and L. Hanna, "Reference model 5 (rm5): Oscillating surge wave energy converter," tech. rep., National Renewable Energy Lab.(NREL), Golden, CO (United States), 2015.
- [4] J. Mi, J. Huang, X. Li, L. Yang, A. Ahmed, R. Datla, M. Folly, M. Hajj, and L. Zuo, "Dual-flap floating oscillating surge wave energy converter: Modelling and experiment evaluation," *IFAC-PapersOnLine*, vol. 55, no. 27, pp. 138–143, 2022.

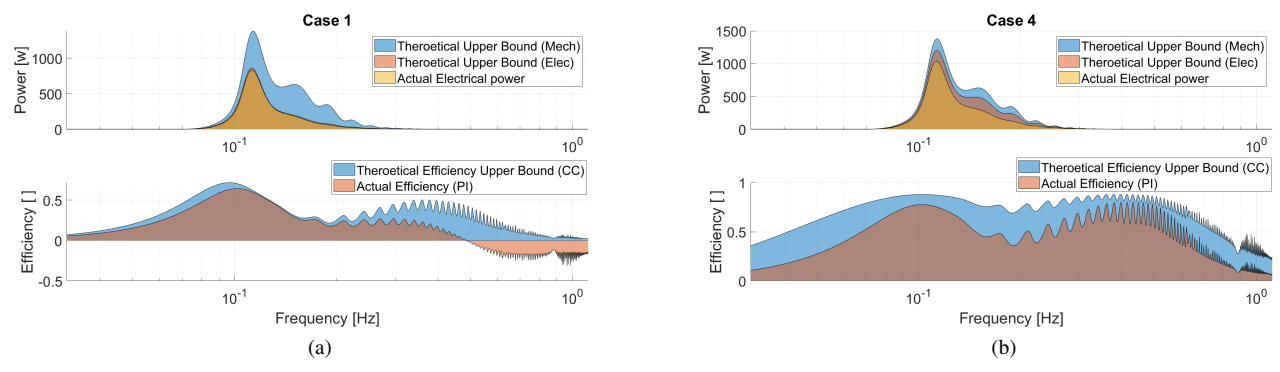


Fig. 8. (a) Power and efficiency for case 1 (without co-optimization); (b) Power and efficiency for case 4 (with co-optimization)

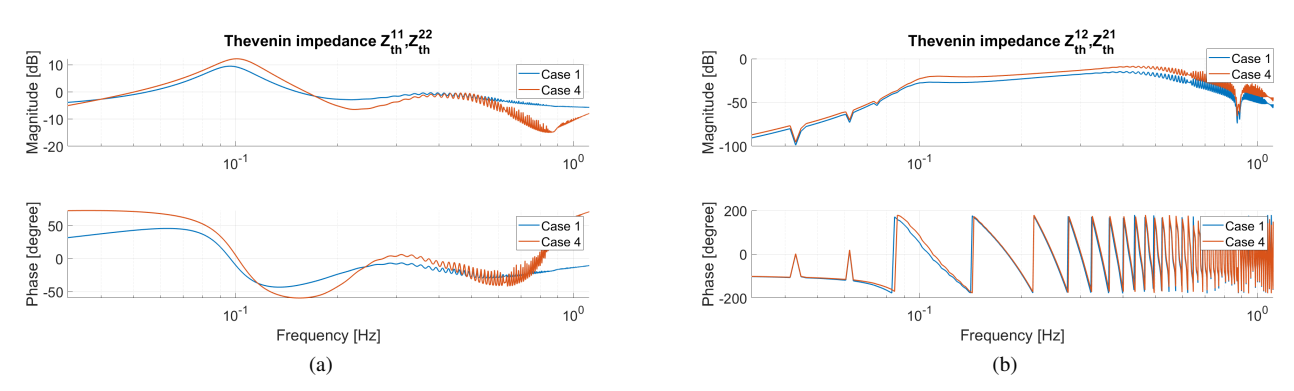


Fig. 9. (a) Diagonal terms of the equivalent WEC output impedance matrix; (b) Off-diagonal terms of the equivalent WEC output impedance matrix

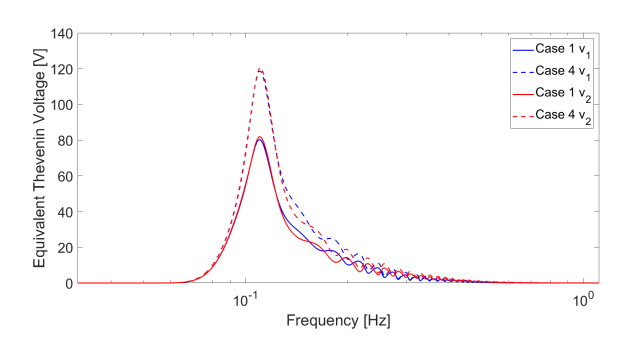


Fig. 10. Equivalent WEC input voltage

- [5] R. G. Coe, G. Bacelli, S. Olson, V. S. Neary, and M. B. Topper, "Initial conceptual demonstration of control co-design for wec optimization," *Journal of Ocean Engineering and Marine Energy*, vol. 6, no. 4, pp. 441– 449, 2020.
- [6] R. Gomes, M. Lopes, J. Henriques, L. Gato, and A. Falcão, "The dynamics and power extraction of bottom-hinged plate wave energy converters in regular and irregular waves," *Ocean Engineering*, vol. 96, pp. 86–99, 2015.
- [7] G. Li and M. R. Belmont, "Model predictive control of sea wave energy converters—part i: A convex approach for the case of a single device," *Renewable Energy*, vol. 69, pp. 453–463, 2014.
- [8] C. Windt, N. Faedo, M. Penalba, F. Dias, and J. V. Ringwood, "Reactive control of wave energy devices—the modelling paradox," *Applied Ocean Research*, vol. 109, p. 102574, 2021.
- [9] G. Bacelli and R. G. Coe, "Comments on control of wave energy converters," *IEEE Transactions on Control Systems Technology*, vol. 29, no. 1, pp. 478–481, 2020.